

ANKLE1 processes chromatin bridges by cleaving mechanically stressed DNA

Received: 9 October 2024

Accepted: 27 October 2025

Published online: 08 December 2025

 Check for updates

Huadong Jiang^{1,2,5}, Fei He^{1,3,5}, Nannan Kong¹, Jie Long³, Yu Ching Poon¹, Rajvee Shah Punatar^{1D}⁴, Zhichun Xu¹, Yuanliang Zhai^{1D}², Stephen C. West^{1D}⁴, Artem K. Efremov^{1D}^{3,6}✉ & Ying Wai Chan^{1D}^{1,6}✉

Chromatin bridges experience significant tension due to spindle fiber pulling and cell migration. Uncontrolled breakage of chromatin bridges by actomyosin contractile forces leads to detrimental consequences. The existence of specialized mechanisms that process chromatin bridges to prevent catastrophic rupture remains uncertain. Here, we uncover a unique property of ANKLE1, a midbody-tethered endonuclease implicated in chromatin bridge processing, in sensing and responding to DNA tension and supercoiling during cell division. Using single-molecule analyses, we found that ANKLE1 specifically cuts supercoiled or mechanically stretched DNA. At higher stretching forces, ANKLE1 cleaves both strands of negatively supercoiled DNA, mirroring conditions in which stretched chromatin bridges lose histones to expose negatively supercoiled DNA. These findings show that ANKLE1 acts as a DNA tension sensor that resolves stretched chromatin bridges. Our study highlights the significance of mechanical forces in DNA bridge processing, enhances our understanding of how cells preserve genome integrity during cell division.

Chromatin bridges primarily arise from dicentric chromosomes resulting from chromosome fusion due to erroneous DNA repair or ectopic recombination between heterologous chromosomes^{1–3}, and the accumulation of unresolved DNA linkages between sister chromatids^{4,5}. These bridges can become trapped by the cleavage furrow in late telophase, activating the Aurora B-dependent abscission checkpoint, which delays cytokinesis and allows a final attempt to process the trapped chromatin^{6–10}. Persistent chromatin bridges continuously stretch and extend due to cell migration, gradually losing nucleosomes and exposing naked DNA^{11–14}. Eventually, they break under actomyosin contractile forces, leading to a range of detrimental consequences such as micronuclei formation, complex genomic rearrangements (e.g., breakage-fusion-bridge (BFB) cycle, chromothripsis, and oncogene amplification), and activation of the GMP-AMP synthase (cGAS)-stimulator of interferon genes (STING) pathway^{15–27}.

C. elegans LEM-3 and its human ortholog ANKLE1 are endonucleases that localize to the midbody and are implicated in processing chromatin bridges at the end of cell division^{15,28–30}. Biochemical studies have shown that LEM-3 and ANKLE1 exhibit nucleolytic activities on supercoiled DNA^{15,31,32}, or various branched DNA species, including flaps, replication forks, and four-way Holliday junctions (HJs)^{30,33,34}. LEM-3 was proposed to resolve DNA bridges by cleaving recombination intermediates, functioning in a genetic pathway parallel to the structure-specific endonucleases SLX-4-SLX-1 and MUS-81²⁹. However, ANKLE1 knockouts in human and mouse cells do not exhibit a reduction in sister chromatid exchange (SCE) levels, disputing a direct role for ANKLE1 in cleaving joint molecules^{15,35}.

In this work, we propose that ANKLE1 operates independently of the resolution pathways and acts directly on chromatin bridges. Furthermore, we show that the DNA cleavage activity of ANKLE1 is enhanced by DNA tension and supercoiling. Its midbody localization

¹School of Biological Sciences, The University of Hong Kong, Pokfulam, Hong Kong SAR, China. ²Division of Life Science, The Hong Kong University of Science and Technology, Clear Water Bay, Hong Kong SAR, China. ³Institute of Systems and Physical Biology, Shenzhen Bay Laboratory, Shenzhen, China. ⁴DNA Recombination and Repair Laboratory, The Francis Crick Institute, London, UK. ⁵These authors contributed equally: Huadong Jiang, Fei He. ⁶These authors jointly supervised this work: Artem K. Efremov, Ying Wai Chan. ✉ e-mail: artem@szbl.ac.cn; gywchan@hku.hk

and unique substrate preference allow it to effectively process stretched chromatin bridges during the final stages of cell division.

Results

ANKLE1 is recruited to the midbody by RACGAP1 to prevent overstretching of bridges

We previously demonstrated that exogenous ANKLE1, when overexpressed, localizes to the midbody in a centrosome-dependent manner¹⁵. To exclude the possibility that this localization was an artifact of overexpression, we employed CRISPR/Cas9 technology to tag endogenous ANKLE1 with GFP in eHAP cells (Fig. 1a). We observed that endogenous ANKLE1-GFP colocalizes with RAC GTPase-activating

protein-1 (RACGAP1) in a bulge-like structure at the midbody, flanked by PLK1 and CEP55 staining (Fig. 1b, c). Importantly, we found that MKLP1 and RACGAP1 could be co-immunoprecipitated with ANKLE1 in telophase (Fig. 1d). The N-terminal Ankyrin repeats domain (1–128 aa) of ANKLE1 is essential for ANKLE1's midbody recruitment¹⁵. We showed that GFP-ANKLE1^{129–615} did not interact with MKLP1 and RACGAP1, while the LEM domain of ANKLE1 was dispensable for midbody localization (Fig. 1e and Supplementary Fig. 1a, b). We further confirmed that ANKLE1^{1–128} is sufficient to localize to the midbody (Supplementary Fig. 1c). Immunoprecipitation revealed that GFP-ANKLE1^{1–128} interacts with overexpressed Myc-RACGAP1 but not with Myc-MKLP1 (Supplementary Fig. 1d, e). Similarly, ANKLE1^{1–128} does not

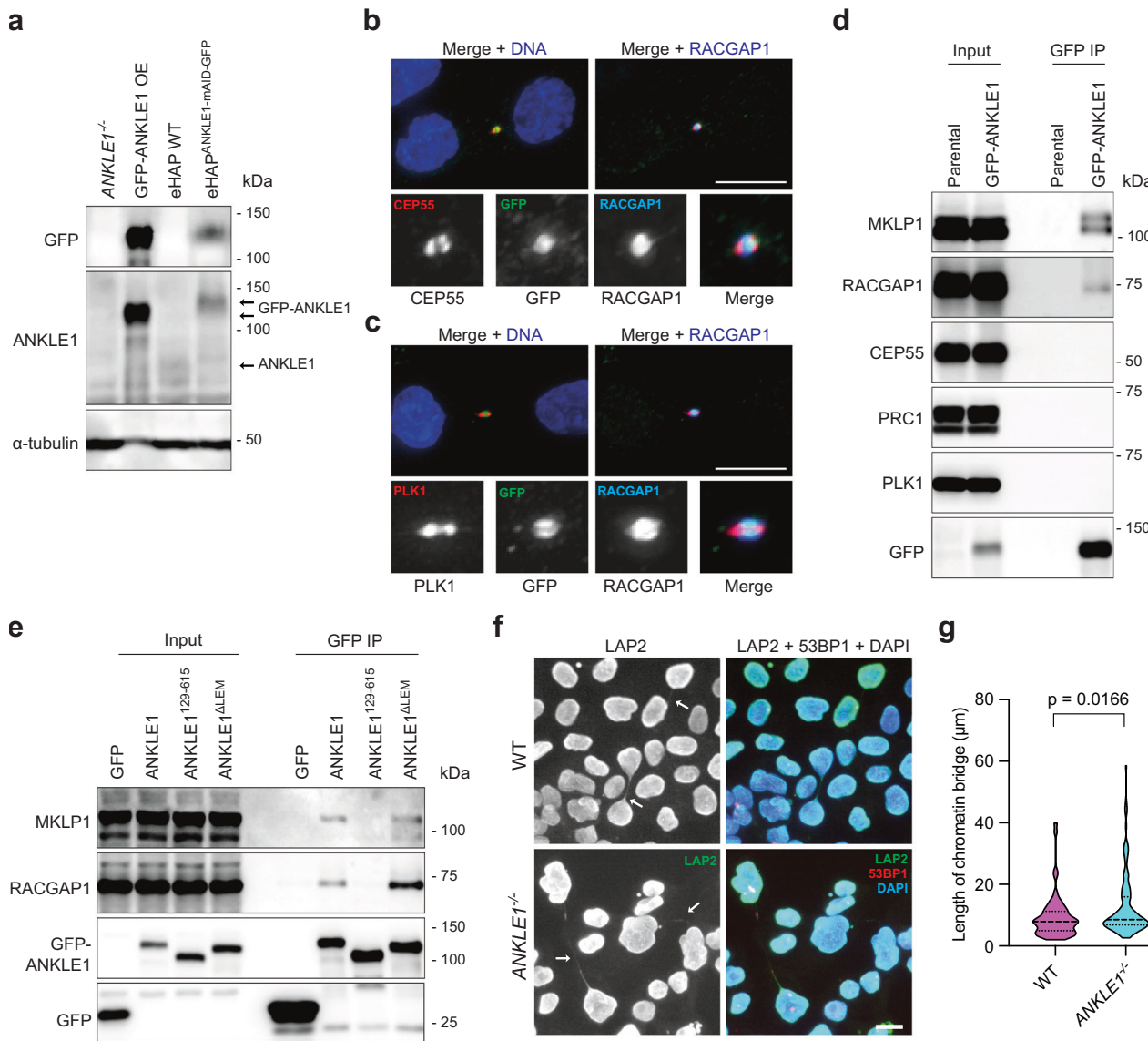


Fig. 1 | ANKLE1 is a midbody-tethered endonuclease for processing chromatin bridges. **a** Cell extracts from *ANKLE1*^{-/-} cells, GFP-ANKLE1 overexpressed (OE) cells, wild-type (WT) eHAP cells, and eHAP cells with ANKLE1 endogenously tagged with a mAID-GFP tag, were analysed by western blotting using the indicated antibodies. **b, c** Cells with ANKLE1 endogenously tagged with a GFP tag were fixed for immunofluorescence. ANKLE1-mAID-GFP (green), CEP55/PLK1 (red), RACGAP1 (blue), and DNA (blue) were visualized. **d** Cell extracts were prepared from telophase-enriched HeLa cells and HeLa cells stably expressing GFP-ANKLE1. GFP-ANKLE1 immunoprecipitates were analysed by western blotting with the indicated antibodies. **e** Cell extracts were prepared from cells expressing GFP, GFP-ANKLE1^{FL},

GFP-ANKLE1^{129–615}, or GFP-ANKLE1^{ΔLEM}. GFP immunoprecipitates were analysed by western blotting with the indicated antibodies. **f** HCT116 WT and *ANKLE1*^{-/-} cells were treated with ICRF-193 for 16 h and fixed for immunofluorescence. LAP2 (green), 53BP1 (red), and DNA (blue) were visualized. Arrows pointing stretched chromatin bridges. Scale bars, 10 μ m. **g** Quantification of the length of chromatin bridges, $n = 59$ and 114 bridges in WT and *ANKLE1*^{-/-} cells, respectively, from three independent experiments. The dotted lines represent the third quartile, median, and first quartile. Statistical significance value was determined with unpaired two-tailed Mann-Whitney test. Source data are provided as a Source Data file.

interact with the N-terminal, middle, and C-terminal region of MKLP1 (Supplementary Fig. 1f, g), but it strongly interacted with a RACGAP1 truncation (Myc-RACGAP⁶¹⁻²⁹²) containing the ECT2-interacting basic region and the cysteine-rich zinc-binding domain (Supplementary Fig. 1h, i). To exclude potential effects of the Myc tag on binding, we also tested interactions using FLAG-tagged full-length and truncated RACGAP1 constructs. Consistently, ANKLE1 interacted with both full-length RACGAP1 and RACGAP1⁶¹⁻²⁹² tagged with a FLAG tag (Supplementary Fig. 1j, k). These results indicate that ANKLE1 is a bona fide midbody protein recruited to the midbody through interaction with RACGAP1.

We measured the length of extended chromatin bridges, visualized by immunostaining of LAP2, in HCT116 wild-type and *ANKLE1*^{-/-} cells and found significantly longer bridges in the *ANKLE1*^{-/-} cells (Fig. 1f, g). These results indicate that ANKLE1 processes chromatin bridges to prevent their overstretching.

Non-overlapping roles for ANKLE1 and GEN1/MUS81 in chromosome segregation

In human mitotic cells, two independent resolution pathways exist: one mediated by GEN1 and the other by the SMX complex, which is composed of SLX1-SLX4, MUS81-EME1, and XPF-ERCC1³⁶⁻⁴⁰. To investigate the genetic relationship of ANKLE1, GEN1, and MUS81, we employed single knockout cells (*ANKLE1*^{-/-}, *GEN1*^{-/-} and *MUS81*^{-/-})¹⁵ and depleted the other nucleases via siRNAs to generate double-deficient cells (Supplementary Fig. 2a). As expected, loss of GEN1 and MUS81, which eliminates the cell's ability to resolve recombination intermediates⁴¹⁻⁴³, resulted in increased formation of both chromatin bridges and ultrafine anaphase bridges (UFBs) (Supplementary Fig. 2b-e). In contrast, loss of both ANKLE1 and GEN1 or MUS81 (*ANKLE1*^{-/-} + siGEN1 and *ANKLE1*^{-/-} + siMUS81) did not result in a higher number of DNA bridges.

Next, we evaluated whether overexpression of ANKLE1 could compensate for the loss of GEN1. *GEN1*^{-/-} cells expressing FLAG-GEN1 or GFP-ANKLE1 were treated with control or MUS81 siRNAs (Supplementary Fig. 3a). Inactivation of both GEN1 and MUS81 resulted in >80% loss of survival. Notably, the expression of exogenous GEN1, but not ANKLE1, significantly reduced cell death (Supplementary Fig. 3b). Additionally, we found that *GEN1*^{-/-} + siMUS81 cells exhibited a substantial increase in the number of G1-specific 53BP1 foci. This increase could be fully rescued by the expression of exogenous GEN1 but not ANKLE1 (Supplementary Fig. 3c, d). Furthermore, we found that overexpression of FLAG-GEN1 could not compensate for the loss of ANKLE1 (Supplementary Fig. 3e-g). These cellular studies indicate that ANKLE1 does not directly participate in the resolution of recombination intermediates and that ANKLE1, GEN1, and MUS81 have non-overlapping roles in chromosome segregation.

Specificity of DNA cleavage by ANKLE1 nuclease

Previously, small synthetic DNA substrates were used to analyze the ability of ANKLE1 to cleave various branched DNA species^{33,34}. To more closely mimic the characteristics of true recombination intermediates, we employed a 1.8 kb long DNA that contained double HJs, in which the two HJs were separated by a maximum of 746 base pairs of homologous sequence, enabling branch migration within the homology region⁴⁴. Whereas this substrate was cleaved efficiently by GEN1⁴⁵, yielding three DNA product bands (~800, ~900, and ~1000 bp), corresponding to the expected crossover (824 and 983 bp) and non-crossover products (903 and 904 bp), no cleavage was observed with ANKLE1 (Fig. 2a, b). Similarly, GEN1 cleaved circular single-stranded φX174 virion DNA (5386 bases) due to the presence of secondary structures susceptible to structure-specific endonuclease cleavage, whereas ANKLE1 was unable to cleave this DNA (Fig. 2c, d).

In contrast to GEN1, however, ANKLE1 was able to cut negatively supercoiled plasmid DNA into mostly nicked circular and a small portion of linear products (Fig. 2e and Supplementary Fig. 4a-c). ANKLE1's ability to cleave plasmid was dependent on superhelicity, as it failed to cut linearized plasmids (Fig. 2e). Furthermore, ANKLE1 did not cleave nicked circular plasmids or linearized plasmids containing a nick (Supplementary Fig. 4c), indicating that ANKLE1 does not cleave the DNA strand opposite a nick.

We hypothesize that ANKLE1 creates a nick on a supercoiled plasmid, releasing superhelical stress, rendering the resulting nicked circular DNA unsuitable for further cleavage due to loss of torsional stress. Experiment using S1 nuclease, which cleaves the DNA strand opposite a nick, demonstrated that ANKLE1-generated nicked circles primarily contained a single nick (Fig. 2f). An alternative explanation for this activity of ANKLE1 is that it targets secondary structures, such as cruciform, formed in the plasmids. To test this, we employed the cruciform-forming sequence containing plasmid pLRbke8^{mut}, which contains an inverted repeat sequences that can be extruded to form a cruciform structure^{46,47}. GEN1, which cuts cruciform by coordinated bilateral cleavage to produce linear products^{45,46}, could not cleave pcDNA4/TO plasmids but readily cleaved pLRbke8^{mut} into linear forms. In contrast, ANKLE1 cleaved both supercoiled plasmids, generating nicked circles (Fig. 3a-d). Additionally, we previously demonstrated that ANKLE1 cleaves various plasmids¹⁵. Together, we conclude that ANKLE1 is an endonuclease with specificity for supercoiled DNA.

Next, we explored ANKLE1's activity on DNA using two C-terminal fragments of ANKLE1: ANKLE1³³¹⁻⁶¹⁵ (containing both the LEM and GIY-YIG domains) and ANKLE1³⁹⁹⁻⁶¹⁵ (containing only the GIY-YIG domain) (Supplementary Fig. 5a-d). As observed with the full-length protein, both fragments cleaved supercoiled plasmids predominantly into nicked circles and a small fraction of linear DNA (Fig. 4a-d), and did not cleave double HJ or φX174 ssDNA (Supplementary Fig. 5e, f). To ensure that the observed activity of ANKLE1 was not due to possible contamination, we purified a catalytically dead version of ANKLE1, ANKLE1^{331-615(Y453A)}, using the same purification protocol (Supplementary Fig. 6a). Importantly, ANKLE1^{331-615(Y453A)} did not cleave supercoiled plasmids (Supplementary Fig. 6b), confirming that the observed cleavage activity was not due to contamination.

ANKLE1 binds specifically to supercoiled DNA

Importantly, electrophoretic mobility shift assays (EMSA) revealed that both ANKLE1³³¹⁻⁶¹⁵ and ANKLE1³⁹⁹⁻⁶¹⁵ readily associated with supercoiled plasmids but not with linearized DNA (Fig. 4e, f). This demonstrates that ANKLE1 specifically binds to supercoiled DNA. The observed upshifts in the EMSA were not due to DNA cleavage, as the addition of 5 mM EDTA completely inhibited ANKLE1's activity (Supplementary Fig. 6c). We also tested ANKLE1^{331-615(Y453A)} in EMSA, which produced similar DNA-binding shifts with supercoiled plasmids (Supplementary Fig. 6d), further confirming that the upshifts were due to binding rather than cleavage. As a control, we conducted EMSA to detect the interaction between BAF (barrier-to-autointegration factor) and supercoiled or linearized plasmids. Clear upshifts of both DNA forms could be observed (Supplementary Fig. 6e), indicating that our assay is sensitive enough to reveal the interaction between proteins and long linear DNA. Interestingly, the absence of the LEM domain in ANKLE1³⁹⁹⁻⁶¹⁵ did not significantly affect ANKLE1's activity or its DNA binding affinity, indicating that the LEM domain is not essential for these functions.

ANKLE1 specifically cuts both strands of negatively supercoiled DNA under tension

The specificity of ANKLE1 for supercoiled plasmids led us to hypothesize that ANKLE1 targets mechanically stressed DNA. To investigate the impact of tension and supercoiling on ANKLE1's nuclease activity, we employed magnetic tweezers to apply stretching forces and

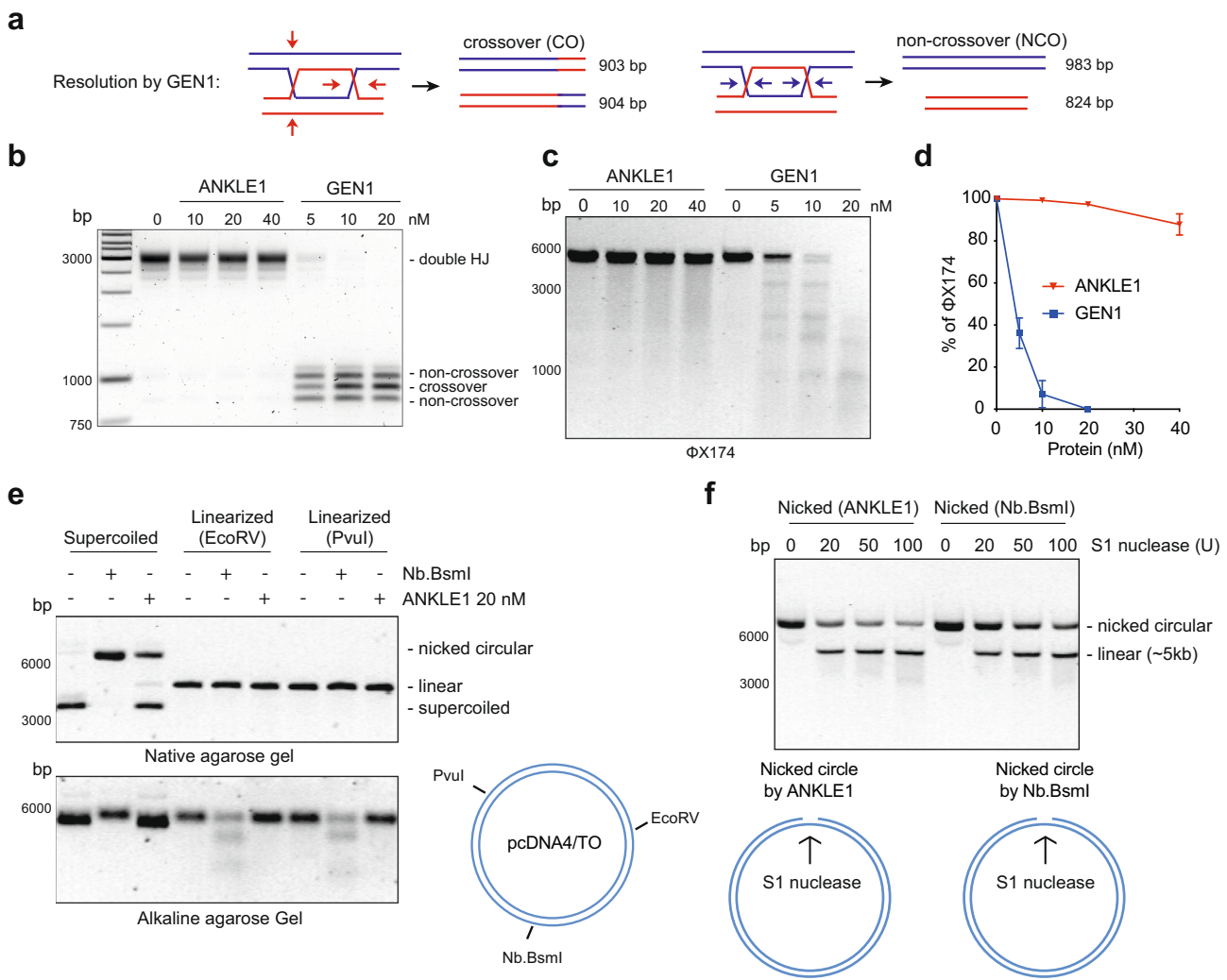


Fig. 2 | ANKLE1 specifically cleaves supercoiled DNA. **a** Schematic diagram indicating the formation of both CO and NCO products arising from GEN1-mediated cleavage of double HJ DNA. **b** Double HJ (3 nM) was incubated with the indicated concentrations of ANKLE1 or GEN1 for 10 min. Products were analysed by agarose gel electrophoresis. **c** As in (b), except that Φ X174 single-stranded circular DNA (1 nM) was incubated with the indicated concentrations of ANKLE1 or GEN1. **d** Quantification of the DNA products, as determined in (c). Plots show mean \pm SD.

from $n = 3$ independent experiments. **e** Supercoiled pcDNA4/TO (0.5 nM), EcoRV-linearized pcDNA4/TO or PvuI-linearized pcDNA4/TO were incubated with ANKLE1 (20 nM) or Nb.BsmI (0.5 μ L) for 5 min. Products were analysed by native (upper) and alkaline (lower) agarose gel electrophoresis. **f** Nicked pcDNA4/TO plasmid DNA (0.5 nM) generated by ANKLE1 or Nb.BsmI were incubated with the indicated amounts of S1 nuclease for 30 min prior to agarose gel electrophoresis. Source data are provided as a Source Data file.

negative supercoiling to a 4100-bp long linear DNA molecule. The DNA was subjected to constant tension of either 0.5 pN or 5 pN, and ANKLE1 was introduced into the experimental chamber (Fig. 5a). These forces are physiologically relevant as previous single-molecule studies showed that forces between 3 and 10 pN can induce nucleosome unfolding^{13,14}, a phenomenon observed in stretched chromatin bridges between daughter cells¹¹, suggesting that the tension experienced by chromatin bridges is comparable to the forces applied in our experiments. At a lower force (0.5 pN), negative supercoiling (superhelical density $\sigma = -0.05$, 20 negative turns) induced plectoneme formation and reduced the DNA end-to-end extension (Fig. 5b). We observed an increase in DNA extension associated with the release of DNA supercoiling as ANKLE1 nicked the DNA (Fig. 5b).

After verifying our setup, we studied the cleavage of negatively supercoiled DNA ($\sigma = -0.1$, 40 negative turns) under a load of 0.5 pN. The half-life of the DNA was determined to be 410 ± 10 s (Fig. 5e green line and Supplementary Fig. 7a). However, this approach cannot be used to measure ANKLE1 activity at a higher force (1.5–5 pN) due to the prevention of plectoneme formation caused by partial melting of

negatively supercoiled DNA, which maintained its end-to-end extension similar to that of torsionally relaxed DNA (Fig. 5c and Supplementary Fig. 8). To discern whether ANKLE1 nicked the DNA under this higher force condition, we applied positive supercoiling (40 positive turns \times 2) to the DNA every 5 min. Intact DNA showed decreased end-to-end distances due to plectoneme formation, whereas those of nicked DNA remained unchanged (Fig. 5c). Intact DNA was then rotated back to the original negatively supercoiled state for subsequent measurements. Remarkably, some beads detached from the surface under higher force, indicating that ANKLE1 cleaved both strands of negatively supercoiled DNA (Fig. 5d). For the remaining attached beads, positive supercoiling was applied every 5 min to check if the DNA became nicked. The fraction of uncleaved DNA was plotted, revealing a half-life of 146 ± 4 s (Fig. 5e red line and Supplementary Fig. 7b). We also plotted the fraction of negatively supercoiled DNA with one or both strands cut by ANKLE1 (Fig. 5f). At a lower force (0.5 pN), ANKLE1 only cleaved one strand of DNA. At a higher force (5 pN), ANKLE1 cleaved both strands of DNA with a half-life of 220 ± 4 s (Fig. 5f and Supplementary Fig. 7c). Collectively, these findings

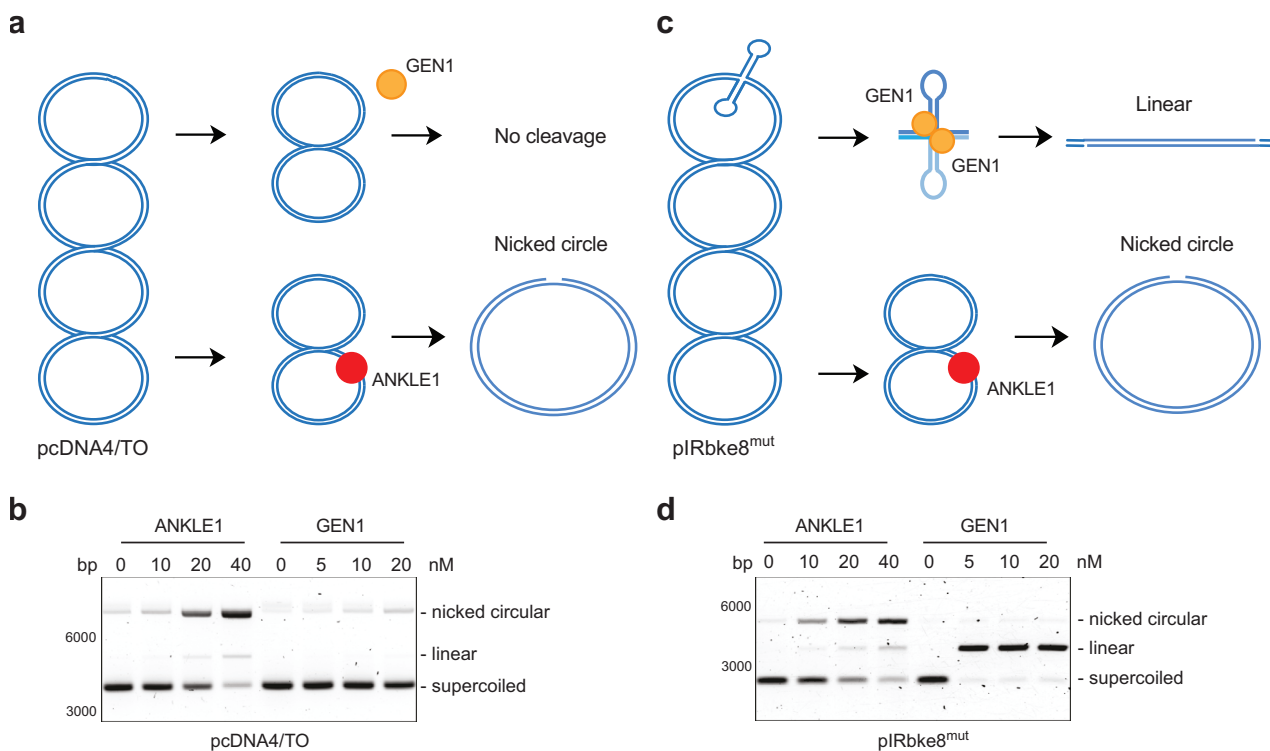


Fig. 3 | ANKLE1 cleaves supercoiled plasmids with or without a cruciform structure. **a** Schematic representation of cleavage assay using supercoiled plasmids without cruciform structure. **b** Plasmid pcDNA4/TO (1 nM) was incubated with the indicated concentrations of ANKLE1 and GEN1. **c** Schematic representation of

cleavage assay using supercoiled plasmids with cruciform structure. **d** Plasmid plRbke8^{mut} (1 nM) was incubated with the indicated concentrations of ANKLE1 and GEN1. Source data are provided as a Source Data file.

demonstrate that ANKLE1's nuclease activity is enhanced by tension and that it specifically cleaves both strands of negatively supercoiled DNA under higher tension, with a faster cleavage rate for the second DNA strand.

We also investigated the effect of lower and higher forces on the cleavage of positively supercoiled (40 positive turns, superhelical density $\sigma = 0.1$) and torsionally relaxed DNA by ANKLE1. Notably, in both cases ANKLE1 only cleaved one strand of the DNA. Higher force increased the cleavage rate of positively supercoiled DNA by ANKLE1 approximately sixfold, reducing the half-life from 780 ± 10 s at 0.5 pN to 130 ± 5 s at 5 pN (Fig. 6a and Supplementary Fig. 7d, e). To measure the fraction of cleaved non-supercoiled DNA, positive supercoiling was applied to the DNA every 5 min. Under lower force, non-supercoiled DNA remained uncleaved by ANKLE1 (cleavage time $\gg 1800$ s, Fig. 6b). However, higher force led to DNA cleavage with a half-life of 360 ± 60 s (Fig. 6b and Supplementary Fig. 7f). In summary, these results show that both tension and supercoiling accelerate the cleavage of the first DNA strand by ANKLE1, while negative supercoiling is necessary for the cleavage of the second strand (Fig. 6c).

To determine whether this tension-sensitive cleavage is specific to ANKLE1, we tested GEN1's ability to cleave stretched DNA in the magnetic tweezers assay. Our results showed that, under either 0.5 pN or 5 pN load, GEN1 did not show a clear ability to cleave negatively supercoiled DNA ($\sigma = -0.1$) (Supplementary Fig. 9). This result supports the conclusion that the enhancement of cleavage activity by tension is specific to ANKLE1.

Analysis of ANKLE1 activity under varying forces and superhelical densities

To determine whether the activity of ANKLE1 continuously increases with tension, we used magnetic tweezers to apply varying forces (0.5,

1.5, 5, and 10 pN) on negatively supercoiled DNA ($\sigma = -0.1$). We observed that the average DNA cleavage time, indicated by bead detachment, significantly dropped from approximately 600 s at 0.5 pN (2 out of 10 beads detached) to about 240 s at 5 pN (12 out of 13 beads detached) (Fig. 6d, e and Supplementary Fig. 10a–d). Notably, increasing the force beyond 5 pN did not further reduce the cleavage time, indicating that a tension of 5 pN is sufficient to fully activate ANKLE1. This was confirmed by the maximum detachment rate of beads at 5 pN (Fig. 6e).

Next, we examined the effect of different superhelical densities on ANKLE1 activity by incubating negatively supercoiled DNA at $\sigma = -0.025$, -0.05 , -0.075 , and -0.1 , maintained under a constant force of 5 pN, with ANKLE1. Our results demonstrated a continuous increase in ANKLE1 cleavage activity with higher negative supercoiling densities (Fig. 6f and Supplementary Fig. 10c, e–g), with over 90% of the beads detached at $\sigma = -0.075$ and -0.1 (Fig. 6g). These findings suggest that both mechanical tension and superhelical density are critical factors in modulating ANKLE1 nuclease activity, with a few piconewtons of tension sufficient to fully activate cleavage and higher negative supercoiling enhancing the enzyme's efficiency.

Discussion

Tension- or supercoiling-sensitive proteins play critical roles in preserving genomic stability by regulating various DNA processes. For example: (i) negative supercoiled DNA recruits adenosine deaminases acting on RNA (ADARs) to edit dsRNA⁴⁸, (ii) high stretching force decreases the rate at which type II topoisomerases can relax DNA⁴⁹, and (iii) the human DNA translocase PICH^{50,51}, and the bacterial RecA recombinase⁵² both exhibit an increased binding affinity for stretched DNA. Our study uncovers a previously unidentified aspect of ANKLE1's role in preserving genome integrity: its role as a

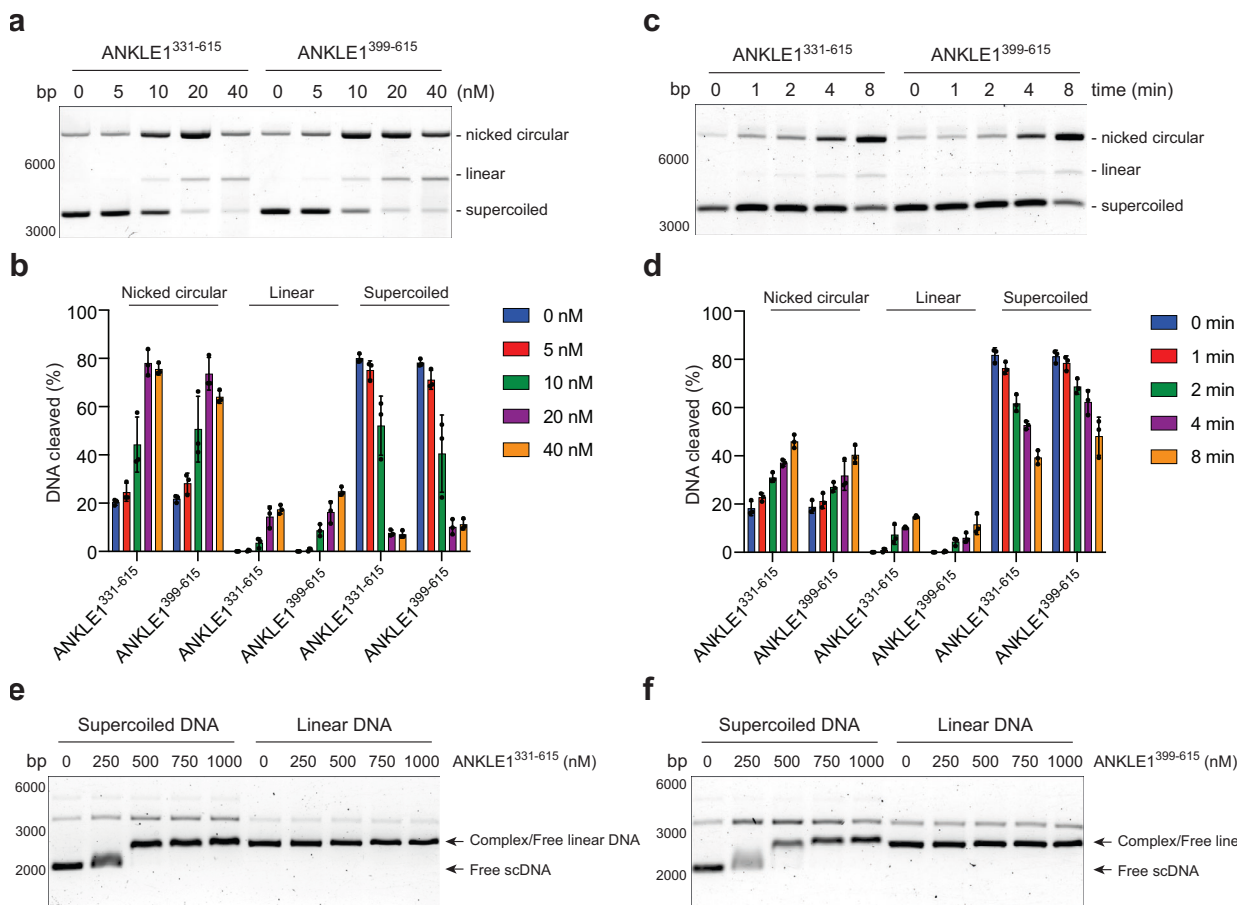


Fig. 4 | ANKLE1 specifically binds to and cleaves supercoiled DNA independent of its LEM domain. **a** A pcDNA4/TO (1 nM) was incubated with the indicated concentrations of ANKLE1³³¹⁻⁶¹⁵ or ANKLE1³⁹⁹⁻⁶¹⁵ for 10 min. **b** Quantification of the DNA products, as determined in (a). Plots show mean \pm SD from $n=3$ independent experiments. **c** pcDNA4/TO (1 nM) was incubated with ANKLE1³³¹⁻⁶¹⁵ or ANKLE1³⁹⁹⁻⁶¹⁵ (20 nM) for the indicated times. **d** Quantification of the DNA products, as

determined in (c). Plots show mean \pm SD from $n=3$ independent experiments. **e, f** ANKLE1³³¹⁻⁶¹⁵ or ANKLE1³⁹⁹⁻⁶¹⁵ were incubated with supercoiled or linearized pUC19 plasmids, and the complexes were analysed by agarose gel electrophoresis. Free DNA and DNA-protein complex are indicated. Source data are provided as a Source Data file.

DNA tension sensor. We have demonstrated that ANKLE1 exhibits increased cleavage activity when acting on negatively supercoiled and mechanically stretched DNA. Interestingly, many restriction enzymes are also influenced by mechanical stretching. For example, a stretching force greater than 0.7 pN strongly inhibits the activity of two-site restriction enzymes but not one-site enzymes⁵³. This inhibition is likely due to the prevention of DNA looping, which is necessary for the enzymes that require interaction at two separate sites to cleave DNA. In contrast, ANKLE1's activity is enhanced by mechanical stress, indicating a different mechanosensitive profile.

Previously, it was shown that the cytoplasmic exonuclease TREX1 acts on bridge DNA when chromatin bridge stretching leads to the loss of nucleosomes¹¹⁻¹⁴. The discovery of ANKLE1's tension-sensitive activity implies that mechanical stretching of chromatin plays a more significant role in chromosome segregation than previously appreciated. DNA wraps around nucleosomes, reducing the DNA linking number by -1.0 to -1.5 per single nucleosome^{54,55}. Given the average DNA length per nucleosome in chromatin (~ 170 – 220 bp), the dissociation of nucleosomes would release negative DNA supercoils with a superhelical density of the order of $\sigma \approx -0.09$ to -0.06 . Thus, the DNA superhelical density $\sigma = -0.1$ used in our single-molecule experiments closely approximates the physiologically relevant range. Therefore, nucleosome unfolding due to chromatin bridge stretching exposes DNA for ANKLE1 cleavage near the midbody. As our magnetic

tweezers assays revealed that ANKLE1 cleaves both strands of stretched, negatively supercoiled DNA, we propose that ANKLE1 can independently resolve chromatin bridges (Fig. 6h). Supporting this hypothesis, our earlier studies showed that *ANKLE1*^{-/-} cells exhibit more severe phenotypes than *TREX1*^{-/-} cells when treated with drugs that induce chromatin bridges¹⁵. Moreover, ANKLE1 has been shown to cleave mitochondrial DNA, which is known to be negatively supercoiled⁵⁶, further reinforcing the idea that ANKLE1 has evolved to target supercoiled/mechanically stressed DNA in specific cellular contexts. This tension/supercoiling sensitivity could be attributed to ANKLE1's specific recognition of local melting induced by negative supercoiling and tension.

In contrast to *C. elegans* LEM-3, human ANKLE1 does not cleave replication/recombination intermediates, emphasizing its unique substrate preference. We propose that in humans, SMX and GEN1 function as the primary nucleolytic resolution pathway that acts on intermediates that escape BTR-mediated HJ dissolution, whereas ANKLE1 has evolved to use its unique tension-recognition properties to cleave any intermediates that persist through anaphase.

Methods

Plasmid construction

To endogenously tag *ANKLE1* with a mini-Auxin-inducible degron (mAID) and a GFP tag, a plasmid expressing sgRNA targeting the last exon of *ANKLE1* was generated. A pair of annealed oligonucleotides

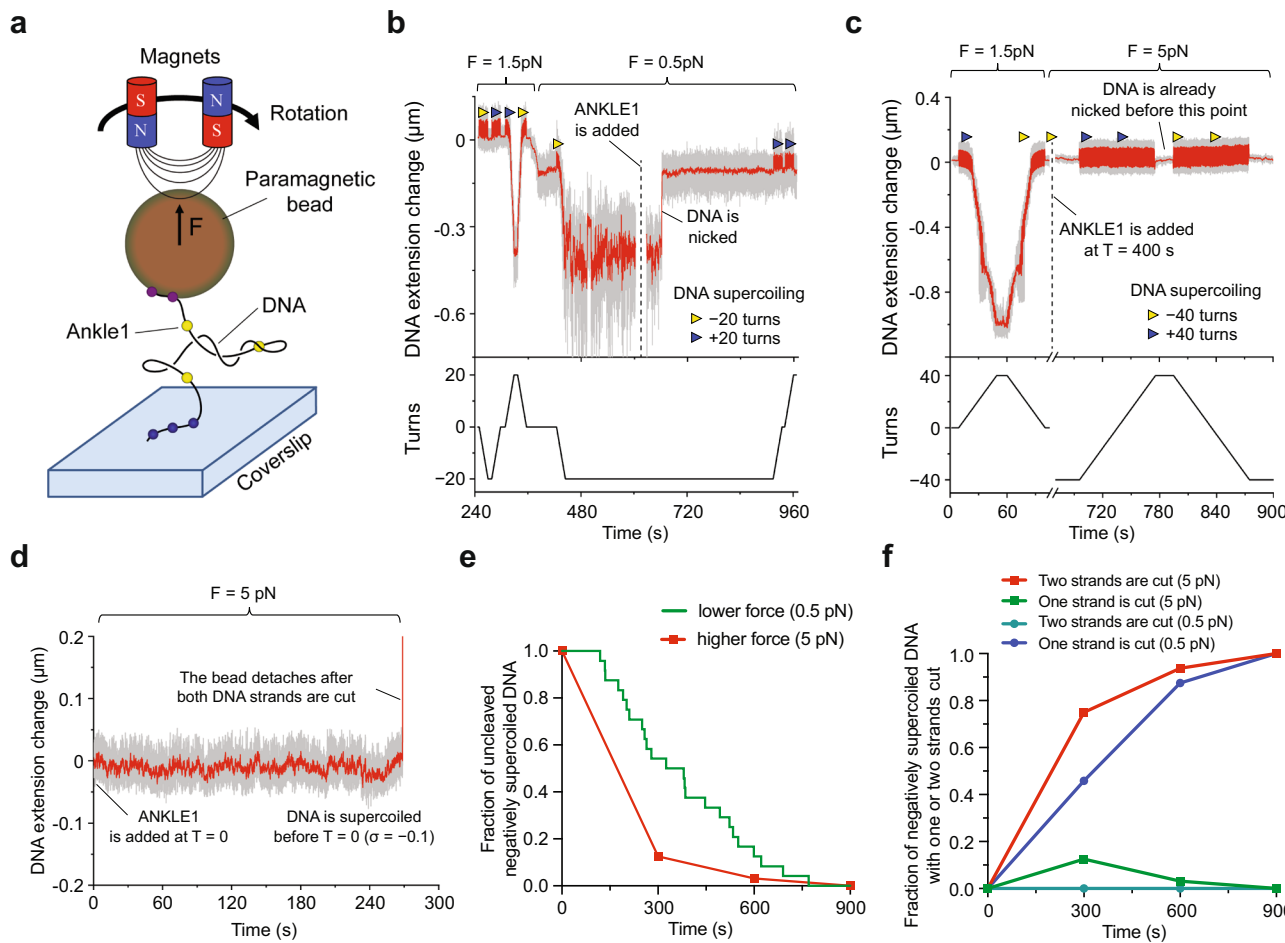


Fig. 5 | ANKLE1 nuclease exhibits greater activity on supercoiled and mechanically stretched DNA. **a** Schematic diagram illustrating the magnetic tweezer experiment setup. A paramagnetic bead attached to DNA was rotated to induce negative or positive supercoiling and plectoneme formation. See text for details. **b** Nicking of negatively supercoiled DNA ($\sigma = -0.05$) by ANKLE1. The magnetic bead attachment to single DNA was first validated by supercoiling of DNA under 1.5 pN load, where DNA extension remained unchanged with negative supercoiling (-20 turns) and decreased with positive supercoiling ($+20$ turns). After validation, the load was reduced to 0.5 pN, negative supercoiling was applied and ANKLE1 was added. Nicking was detected by an increase in DNA extension due to the release of supercoiling. Post-nicking, DNA extension remained unchanged with positive rotation of the bead. The upper plot shows the DNA extension change vs time, and the lower plot shows turns vs time. **c** Nicking of negatively supercoiled DNA ($\sigma = -0.1$) by ANKLE1 under 5 pN load. After validation of the DNA bead under 1.5 pN load, the load was increased to 5 pN, negative supercoiling (-40 turns) was applied and ANKLE1 was added. DNA nicking by ANKLE1 was tested every 5 min by positively supercoiling DNA. The upper plot shows the DNA extension change vs time, and the lower plot shows turns vs time. **d** Cleavage of both strands of the negatively supercoiled DNA by ANKLE1 under 5 pN load, as detected by the complete detachment of the magnetic bead and its movement toward the magnetic field source. **e** Graph showing the fraction of uncleaved negatively supercoiled DNA ($\sigma = -0.1$) over time. $n = 32$ and 24 for DNA under higher and lower forces, respectively. **f** Graph showing the fraction of negatively supercoiled DNA with one or two strands cut under lower and higher forces. Source data are provided as a Source Data file.

DNA ($\sigma = -0.1$) by ANKLE1 under 5 pN load. After validation of the DNA bead under 1.5 pN load, the load was increased to 5 pN, negative supercoiling (-40 turns) was applied and ANKLE1 was added. DNA nicking by ANKLE1 was tested every 5 min by positively supercoiling DNA. The upper plot shows the DNA extension change vs time, and the lower plot shows turns vs time. **d** Cleavage of both strands of the negatively supercoiled DNA by ANKLE1 under 5 pN load, as detected by the complete detachment of the magnetic bead and its movement toward the magnetic field source. **e** Graph showing the fraction of uncleaved negatively supercoiled DNA ($\sigma = -0.1$) over time. $n = 32$ and 24 for DNA under higher and lower forces, respectively. **f** Graph showing the fraction of negatively supercoiled DNA with one or two strands cut under lower and higher forces. Source data are provided as a Source Data file.

(target sequence: AGGCCCGGGCTGAGTCCTG) was cloned into pX330 vector (Addgene #42230) according to the published protocol⁵⁷. Two donor plasmids (pUC-SP-ANKLE1-mAID-Clover) for endogenous tagging were based on pMK289 (Addgene #72827) and constructed according to the previous protocol⁵⁸. In brief, a plasmid pUC-AP-ANKLE1 with ~500-bp homology arms was synthesized from gene synthesis (ATCG). The fragment of mAID-Clover-Neo was cut out from pMK289 by BamHI (New England Biolabs) and cloned into pUC-SP-ANKLE1 to generate pUC-SP-ANKLE1-mAID-Clover (Neo). pUC-SP-ANKLE1-mAID-Clover (Zeo) was also generated by replacing Neo-resistant gene to Zeocin-resistant gene. Full-length ANKLE1, ANKLE1¹²⁹⁻⁶¹⁵, and ANKLE1¹⁻¹²⁸ were generated as described¹⁵. ANKLE1^{ΔLEM} was generated by PCR and cloned into a pcDNA3.1+/-N-eGFP and a pcDNAS/FRT/TO (Thermo Fisher) vectors. The MKLP1 and RACGAP cDNA cloned in pCMV3-N-FLAG were purchased from Sino Biological (Cat. No. HG19110-NF and HG18716-NF, respectively). The various MKLP1/RACGAP1 truncations were generated by PCR and

cloned into a pcDNA3.1-3 × Myc or pcDNAS-3 × FLAG vectors. GEN1-3 × FLAG was cloned into a pcDNA4/TO (Thermo Fisher) vector as described previously⁵⁹. The sgRNA vectors for generating ANKLE1^{-/-}, MUS81^{-/-}, and GEN1^{-/-} cells were cloned in the px459 (Addgene #62988) or pX330 vectors as described previously¹⁵. ANKLE³³¹⁻⁶¹⁵ and ANKLE¹³⁹⁹⁻⁶¹⁵ were generated by PCR from codons optimized ANKLE1 for *E. coli* expression (GeneArt Gene Synthesis) and cloned into a pCold TF vector (Takara), carrying an N-terminal trigger factor chaperone and a 6 × His tag. ANKLE^{331-615(Y453A)} was generated using QuikChange lightning multi-site directed mutagenesis (Agilent). The cDNA of BAF (Sino Biological, Cat. No. HG16240-G) was cloned into a pET28a (Merck Millipore) vector with a N-terminal 6 × His tag.

Biological resources

HeLa and HCT116 cells were obtained from ATCC. eHAP cells were obtained from Horizon Discovery. Flp-IN T-REx 293 cells were obtained from Thermo Fisher. U2OS Flp-In T-Rex cells was a gift from Erich Nigg

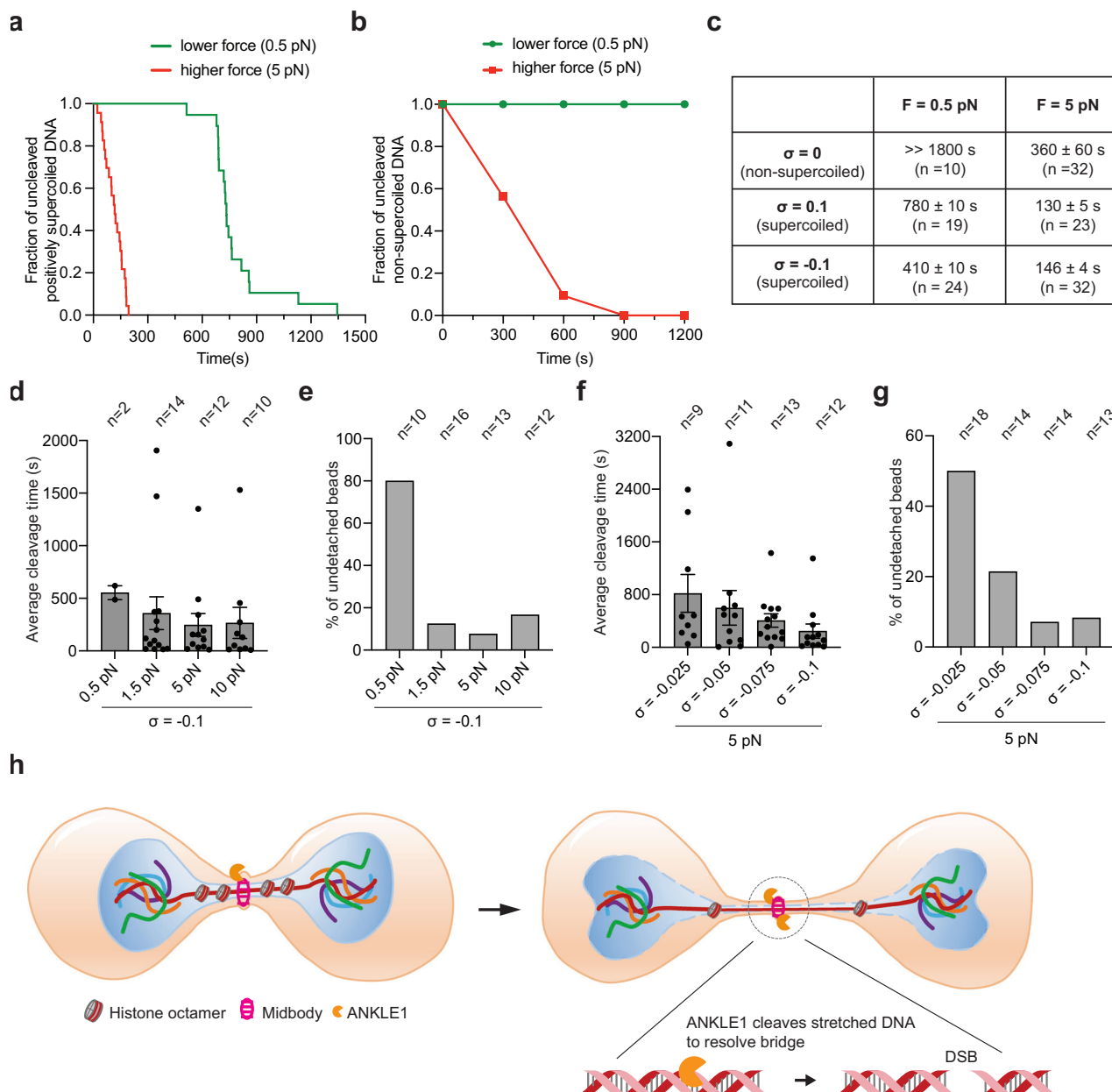


Fig. 6 | The effect of varying forces and superhelical densities on the activity of ANKLE1. **a** Graph showing the fraction of uncleaved positively supercoiled DNA ($\sigma = 0.1$) over time. $n = 23$ and 19 for DNA under higher and lower forces, respectively. **b** Graph showing the fraction of uncleaved non-supercoiled DNA over times. $n = 32$ and 10 for DNA under higher and lower forces, respectively. **c** Table summarizing the half-lives of uncleaved DNA when incubated with ANKLE1. The half-lives were calculated by fitting the data to an exponential decay function (see Supplementary Fig. 7). **d** Bar graph showing the average cleavage time of negatively supercoiled DNA ($\sigma = -0.1$) under the indicated forces. The number of beads that detached from the surface is indicated in the graph. Error bars represent the

mean \pm SEM. **e** A bar graph showing the percentage of beads detached from the surface as in (d). The number of total beads examined is indicated in the graph. **f** Bar graph showing the average cleavage time of negatively supercoiled DNA ($\sigma = -0.025, -0.05, -0.075, -0.1$) under a tension of 5 pN. The number of beads that detached from the surface is indicated in the graph. Error bars represent the mean \pm SEM. **g** Bar graph showing the percentage of beads detached from the surface as in (f). The number of total beads examined is indicated in the graph. **h** Model of how ANKLE1 is involved in resolving stretching chromatin bridges. See text for the details. Source data are provided as a Source Data file.

(University of Basel). eHAP cells were cultured in IMDM medium (Thermo Fisher). All other cell lines were cultured in DMEM medium (Thermo Fisher). Cells were cultured in medium supplemented with 10% fetal bovine serum (Cat No. 10270106, Thermo Fisher) and penicillin-streptomycin (100 U/mL, Thermo Fisher) at 37 °C in 5% CO₂. To generate eHAP^{ANKLE1-mAID-GFP} cell line, eHAP cells were transfected with pX330-sgANKLE1 targeting the last exon and the two donor plasmids using Lipofectamine 2000 (Thermo Fisher) according to the manufacturer's instructions. Colonies resistant to both geneticin and

zeocin were picked and expanded. To generate U2OS cells expressing ANKLE1^{WT} and ANKLE1^{ΔLEM}, U2OS Flp-In T-REx cells were co-transfected with the pcDNA5/FRT/TO plasmids encoding ANKLE1^{WT} or ANKLE1^{ΔLEM} and pOG44 plasmids that encode Flp recombinase (1:9 ratio) using Lipofectamine 2000. Hygromycin-resistant colonies were picked and expanded. Protein expression was induced by adding doxycycline (1 µg/mL). To generate stable HeLa and HCT116 cells expressing different constructs of ANKLE1 or GEN1, cells were transfected with pcDNA3.1+ or pcDNA4/TO plasmids encoding the protein of interest

using Lipofectamine 2000, and geneticin- or zeocin-resistant colonies were picked and expanded.

siRNA transfection

siRNA transfection was performed using Lipofectamine RNAiMAX (Thermo Fisher). Cells were seeded one day before siRNA treatment and transfected with 25 nM of siRNA. The following siRNAs⁴¹ were used: control siRNA: UAAUGUAUUGGAACGCAUA; GEN1 siRNA: GUAAAGACCUGCAAUGUUA; MUS81 siRNAs: CAGCCCUGGGUGGAUC-GAUA and CAUUAAGUGUGGGCGUCUA. siRNAs were purchased from GenePharma.

Cell extracts, western blotting, and immunoprecipitation

Cell lysates were prepared by lysing cells in Tris-lysis buffer (50 mM Tris-HCl pH 7.5, 150 mM NaCl, 0.5% NP-40, 1 mM EDTA, 1 mM DTT) supplemented with protease inhibitors (Thermo Fisher). The lysates were incubated on ice for 30 min and then cleared by centrifugation (18,000 × g for 30 min at 4 °C). For western blotting of ANKLE1, RIPA buffer (50 mM Tris-HCl pH 7.5, 150 mM NaCl, 1% Triton ×-100, 0.5% sodium deoxycholate, 0.1% SDS, and 5 mM EDTA) was used to lyse the cells. Protein concentrations were determined using Bradford Assay and equal amounts of total proteins were loaded in each lane of the SDS gel. Proteins were transferred to nitrocellulose membranes (Bio-Rad). After blocking with 5% non-fat milk in PBST (PBS + 0.1% Tween 20), membranes were incubated with primary and secondary antibodies sequentially. Proteins were detected by SuperSignal West Pico Chemiluminescent Substrate (Thermo Fisher) and the Bio-Rad ChemiDoc MP Imaging System. For immunoprecipitation, telophase cells were enriched by nocodazole shake-off and released into fresh medium for 1.5 h. Enrichment of telophase cells were validated by microscopy analysis. Cell extracts (~1 mg) were incubated with GFP-trap beads (Chromotek) at 4 °C with gentle rotation for 1 h. The beads were washed extensively with Tris-lysis buffer, and boiled directly in 2× SDS sample buffer at 95 °C for 5 min.

Immunofluorescence and microscopy

Immunofluorescence was carried out as described previously⁶⁰. In brief, cells were grown on coverslips and fixed with PTEMF buffer (20 mM PIPES pH 6.8, 0.2% Triton ×-100, 10 mM EGTA, 1 mM MgCl₂, and 4% formaldehyde) for 10 min. Fixed cells were blocked with 3% BSA in PBS for 30 min and then incubated with primary antibodies diluted in 3% BSA in PBS for 1 h, washed with PBS and incubated with secondary antibodies diluted in 3% BSA in PBS for 1 h. DNA was stained with DAPI (10 µg/mL). The coverslips were washed twice with PBS and then mounted with Prolong Diamond antifade mountant (Thermo Fisher) on microscope slides. Images were acquired using a Nikon Ti60 microscope equipped with DS-Ri2 camera under 40× objective by NIS-Elements D (5.30.03) software, or a DeltaVision Ultra microscope (Cytiva Life Sciences) equipped with a PlanApo 60×/1.50 oil immersion objective and a CoolSNAP HQ camera (Photometrics) using SoftWoRx DV AcquireUltra (1.2.3) software. DeltaVision images at single focal planes were processed with a deconvolution algorithm, and optical sections were projected using maximum intensity projection into one picture using SoftwoRx (7.2.2). Images were adjusted using Adobe Photoshop 2023. The length of chromatin bridges was measured by Fiji (ImageJ 2.14.0).

Reagents

Geneticin (500 µg/mL), hygromycin (100 µg/mL), zeocin (50 µg/mL), blasticidin (5 µg/mL), and puromycin (0.5 µg/mL) were obtained from Thermo Fisher. Nocodazole, ICRF-193, and doxycycline were obtained from Sigma-Aldrich. The following enzymes were obtained from New England Biolabs: BamHI (R3136), EcoRI (R0101), Pvul (R3150), EcoRV (R3195), HindIII (R0104), KasI (R0544), Nb.BsmI (R0706), Nt.BspQI (R0644), and T4 DNA ligase (M0202). S1 nuclease (EN0321) was

obtained from Thermo Fisher. Proteins were detected by western blotting or immunofluorescence using the following primary antibodies: rabbit anti-ANKLE1 (1:500, raised against full length ANKLE1 purified in denatured condition)¹⁵, rabbit anti-GFP (1:5000, Abcam ab290), mouse anti-GFP (1:1000, Roche 11814460001), mouse anti-α-tubulin (1:5000, Sigma 00020911), rabbit anti-Aurora B (1:2000, Abcam ab2254), mouse anti-CEP55 (1:500, Santa Cruz Biotechnology sc-374051), mouse anti-PRC1 (1:500, Santa Cruz Biotechnology sc-376983), mouse anti-PLK1 (1:1000, Santa Cruz Biotechnology sc-17783), goat anti-RACGAP1 (1:400, Abcam ab2270), mouse anti-MKL1 (1:200, Santa Cruz Biotechnology sc-390113), rabbit anti-PICH (1:100, Cell Signaling 8886S), mouse anti-RPA (1:1000, Abcam ab2175), rabbit anti-53BP1 (1:1000, Abcam ab36823), mouse anti-Cyclin A (1:200, Santa Cruz sc-271682), rabbit anti-GEN1 (1:500, raised against GEN1⁸⁹⁰⁻⁹⁰⁸)⁴⁶, mouse anti-MUS81 (1:1000, Santa Cruz Biotechnology sc-47692), mouse anti-FLAG M2 (1:1000, Sigma F1804), mouse anti-Myc 9E10 (1:1000, Thermo Fisher MA1-980), and mouse anti-LAP2 (1:2000, BD Biosciences 611000). For western blotting, primary antibody detection was performed using HRP-conjugated goat anti-mouse, goat anti-rabbit, and rabbit anti-goat antibodies (1:2000, Bio-Rad 1706515, 1706516, 1721034). For immunofluorescence, primary antibody detection was performed using secondary antibodies conjugated to Alexa Fluor 488, Alexa Fluor 546, Alexa Fluor 555, and Alexa Fluor 647 against rabbit, mouse, or goat immunoglobulin heavy and light chain (1:2000, Thermo Fisher A11001, A11070, A11010, A31570, and A21447).

Clonogenic cell survival assay

Cells were first transfected with siRNAs for 24 h. 200 cells were seeded in 6-well plates. Cell medium was changed every 3 days. Colonies were stained for ~2 min with 40 mg/mL crystal violet solution (Sigma-Aldrich) containing 20% ethanol, and then washed twice with water.

Protein expression and purification

GEN1 and full-length ANKLE1 were purified as described previously^{15,45}. To purify ANKLE1³³¹⁻⁶¹⁵, ANKLE1^{331-615(Y453A)}, and ANKLE1³⁹⁹⁻⁶¹⁵ proteins, the plasmids were transformed into One Shot™ BL21 Star™ DE3 *E. coli* competent cells (Thermo Fisher). Transformed BL21 cells were grown in LB medium at 37 °C until the OD₆₀₀ of the culture reached ~0.6. The culture was quickly cooled down to 15 °C (in ice water for 30 min). The expression of ANKLE1 was induced by addition of 0.5 mM of isopropyl β-D-thiogalactoside (IPTG) (Thermo Fisher) and incubated at 15 °C with shaking for 24 h. Cells were harvested and resuspended in lysis buffer (25 mM HEPES pH 7.5, 500 mM NaCl, 10% glycerol, 0.2% NP-40, 0.5 mg/mL lysozyme, 10 mM imidazole, 1 mM phenylmethanesulfonyl fluoride (PMSF), and protease inhibitor tablets (Thermo Fisher)) and then disrupted in a high-pressure homogenizer (Union-Biotech). The lysate was clarified by centrifugation at 18,000 × g for 1 h at 4 °C. The supernatant was incubated with Ni-NTA agarose beads (Qiagen) for 2 h at 4 °C. The beads were washed five times in wash buffer (25 mM HEPES pH 7.5, 500 mM NaCl, 10% glycerol, 0.2% NP-40, and 30 mM imidazole). Proteins were eluted with His elution buffer (25 mM HEPES pH 7.5, 100 mM NaCl, 10% glycerol, 0.2% NP-40, and 300 mM imidazole). To further purify the proteins, the eluate (~3 mL) was loaded on a HiTrap Q HP anion exchange chromatography column (Cytiva), then eluted from the column with a continuous gradient of NaCl from 100 mM to 1 M in 30 column volumes using a AKTA pure system (GE Healthcare). The fractions were collected and analysed by SDS-PAGE followed by Coomassie blue staining. Peak fractions containing pure ANKLE1 proteins were pooled. The proteins were then aliquoted, frozen in liquid nitrogen, and stored in -80 °C freezer. For purification of BAF, the pET28a-6xHis-BAF plasmids were transformed into One Shot™ BL21 Star™ DE3 *E. coli* cells. Cells were grown at 37 °C and protein expression was induced with 0.5 mM IPTG at OD₆₀₀ of ~0.8. After 2 h, cells were harvested and resuspended in lysis buffer (25 mM HEPES pH 7.5, 150 mM NaCl, 1 mg/ml lysozyme) with 1 mM PMSF and protease

inhibitors, then sonicated. Lysates were centrifuged for 30 min at 18,000 $\times g$, and the supernatant was discarded. The pellet containing BAF was solubilized in buffer (25 mM HEPES pH 7.5, 150 mM NaCl, 25 mM imidazole) with 6 M guanidinium chloride and agitated for 1 h at 4 °C. The lysate was centrifuged again, and the supernatant was incubated with Ni-NTA agarose beads for 2 h at 4 °C. The beads were washed extensively with solubilization buffer, and the protein was eluted with solubilization buffer containing 400 mM imidazole. The eluted protein was dialyzed overnight in buffer B (100 mM potassium phosphate pH 6.5, 5 mM EDTA, 200 mM NaCl). The dialyzed proteins were supplemented with 100 mM DTT and incubated for 2 h at 40 °C to reduce disulfide bonds. Proteins were then loaded onto a Superdex 200 10/300 GL size exclusion chromatography column (Cytiva) run with buffer B. Fractions containing monomeric BAF were pooled, aliquoted, frozen in liquid nitrogen, and stored at -80 °C.

Nuclease assay

Different DNA substrates were incubated with ANKLE1 or GEN1 in cleavage buffer (50 mM Tris-HCl pH 8.0, 1 mM DTT) at 37 °C. For ANKLE1, the cleavage buffer was supplemented with 1 mM or 10 mM MnCl₂. For GEN1, the cleavage buffer was supplemented with 1 mM MgCl₂. Φ X174 single-stranded circular virion DNA was purchased from New England Biolabs (N3023). The double Holliday junction substrate was generated as described⁴⁴. Cruciform extrusion of plasmid pIRbk8^{mut} was stimulated by incubation for 90 min at 37 °C in 50 mM Tris-HCl pH 7.5, 50 mM NaCl, and 0.1 mM EDTA. Digestion with EcoRI was used to determine the efficiency of cruciform extrusion. DNA products (in 10 μ L reaction volume) were deproteinized by the addition of 2.5 μ L of 5× stop buffer (100 mM Tris-HCl pH 7.5, 50 mM EDTA, 2.5% SDS, and 10 mg/mL proteinase K) and incubation for 60 min at 37 °C. The products were analysed by 0.8% agarose gel electrophoresis running in 1× TBE buffer (90 mM Tris base, 90 mM boric acid, 2 mM EDTA), stained with 1:10,000 SYBR Gold (Thermo Fisher) and imaged with a Gel Doc 2000 System (Bio-Rad). Reaction products were quantified using Image Lab 6.1 software (Bio-Rad). To analyse the reaction products by alkaline agarose gel electrophoresis, a 1% alkaline agarose gel was prepared by first dissolving agarose in boiled water, followed by addition of 50× alkaline buffer (1.5 M NaOH and 50 mM EDTA) until 1% agarose in 1× alkaline gel buffer was made. Deproteinized DNA samples were mixed with an equal volume of 2× alkaline loading buffer (60 mM NaOH, 2 mM EDTA, 20% Ficoll 400, 0.06% Bromocresol Green) and run into 1% alkaline agarose gel in 1× alkaline gel buffer (30 mM NaOH and 1 mM EDTA).

Electrophoretic mobility shift assays (EMSA)

EMSA was carried out for 15 min at room temperature by mixing different concentrations of ANKLE1³³¹⁻⁶¹⁵, ANKLE1¹³⁹⁹⁻⁶¹⁵, ANKLE1^{331-615(Y453A)} or BAF with 0.5 nM of supercoiled or linearized pUC19 plasmids in 10 μ L binding buffer (50 mM Tris-HCl pH 8.0, 0.5 mM DTT, 100 μ g/mL BSA, 50 mM NaCl, 5 mM EDTA, 5% glycerol). Complexes were separated by 0.8% TBE agarose gel in per-chilled 0.5× TBE buffer, stained with 1:10,000 SYBR Gold and imaged with a Gel Doc 2000 System (Bio-Rad).

DNA preparation for magnetic tweezers experiments

DNA is prepared as described previously^{61,62}. In brief, 6.5 kb DNA constructs were used, which were assembled from three different parts -4.1 kb middle part dsDNA, and 1 kb biotin-labeled and digoxigenin-labeled dsDNA end segments (handles) that were used to attach the DNA constructs to the glass surface coated with anti-digoxigenin antibodies at one end and streptavidin-coated paramagnetic bead at the other end. The middle 4.1 kb part was obtained by digestion of pcDNA3.1(+) plasmid by HindIII and KsI restriction enzymes (New England Biolabs). As for the biotin- and digoxigenin-labeled DNA handles, they were

synthesized using pcDNA3.1(+) plasmid as a template in a PCR reaction containing a mixture of dATP, dCTP, dGTP nucleotides, and biotin-16-dUTP and digoxigenin-11-dUTP nucleotides (Roche), respectively. Biotin-labeled DNA was then digested by KsI and digoxigenin-labeled DNA handle was digested by HindIII. After DNA gel purification, all the three DNA parts were ligated together using T4 ligase (New England Biolabs) overnight at 16 °C.

Magnetic tweezers experiments

A commercially available magnetic tweezers and microscopy instrument (BioPSI) was used. Magnetic tweezers experiments were performed as described previously^{61,62}. In brief, flow chambers of 40 - 50 μ L volume were used, which were prepared from two #1 glass coverslips spaced by two adhesive strips (Grace Bio-Labs). The bottom coverslip used in these chambers, was pretreated in a plasma chamber and coated with dopamine hydrochloride (Macklin). After the chamber assembly, anti-Digoxigenin Fab fragments (Roche) were covalently bound to the dopamine hydrochloride. To avoid non-specific binding of DNA to the surface of the flow chambers, the chamber working surface was blocked with 2% BSA solution in 1× PBS buffer by incubating it overnight at 4 °C. On the day of experiment, the DNA constructs were washed into the flow chamber at 0.1 - 0.2 ng/ μ L concentration in the washing buffer (50 mM KCl, 10 mM Tris, 1 mM MgCl₂, pH 7.5) and incubated for 10 min at room temperature. After that, 1 μ m sized magnetic beads (Invitrogen) coated with streptavidin were added to the chamber and incubated for another 10 min. Unbound DNA and magnetic beads were then removed by washing the chamber with the washing buffer. After DNA constructs capable of supercoiling were found in the flow chamber, the washing buffer was replaced with the working buffer (50 mM Tris, 1 mM DTT, 10 mM MnCl₂, pH 8.0). Experiments were conducted at 25 °C. To apply a constant load and to supercoil the DNA constructs, a pair of Neodymium magnets mounted onto a translational and rotational micromanipulator stage were used, which allowed a full 3D control of the magnets' position/rotation angle. The magnitude of the stretching force was controlled by changing the distance between magnets and the flow chamber containing the DNA molecules attached to magnetic beads. Winding and unwinding of the DNA constructs attached to magnetic beads was done by rotating the magnet in counterclockwise and clockwise direction, respectively.

Statistics and reproducibility

Sample sizes were determined based on previous experience to obtain statistical significance and reproducibility. All measurements were taken from distinct samples. Error bars represent mean \pm standard deviation (SD) from at least $n = 3$ independent experiments, unless otherwise specified. The half-lives of the DNA were calculated by fitting the data to an exponential decay function using OriginPro 2021. For data assumed to be normally distributed, an unpaired two-tailed *t*-test was used. For data not assumed to be normally distributed, a Mann-Whitney test was performed. Statistical tests were conducted using GraphPad Prism 10 software. A *p*-value of less than 0.05 was considered statistically significant. Exact *p*-values were indicated above the graphs, except when *p* < 0.0001 and *p* > 0.05 (not significant, ns). Each experiment was repeated at least three times, with the exception of the those presented in Figs. 1d, e and 4e, f, Supplementary Fig. 1g, i, k (two experiments were performed) and Figs. 1a-c, 2e, f, and 3b, d, and Supplementary Figs. 1b-e, j, 2a, 3a, e, 4c, 5b, d-f, 6a-e, 8, and 9 (one experiment was performed).

Reporting summary

Further information on research design is available in the Nature Portfolio Reporting Summary linked to this article.

Data availability

All data and materials reported in this study are available upon request from the corresponding authors. Source data are provided with this paper as a Source Data file. Source data are provided with this paper.

References

1. de Lange, T. Shelterin: the protein complex that shapes and safeguards human telomeres. *Genes Dev.* **19**, 2100–2110 (2005).
2. Mizuno, K., Miyabe, I., Schalbetter, S. A., Carr, A. M. & Murray, J. M. Recombination-restarted replication makes inverted chromosome fusions at inverted repeats. *Nature* **493**, 246–249 (2013).
3. Mizuno, K., Lambert, S., Baldacci, G., Murray, J. M. & Carr, A. M. Nearby inverted repeats fuse to generate acentric and dicentric palindromic chromosomes by a replication template exchange mechanism. *Genes Dev.* **23**, 2876–2886 (2009).
4. Bizard, A. H. & Hickson, I. D. Anaphase: a fortune-teller of genomic instability. *Curr. Opin. Cell Biol.* **52**, 112–119 (2018).
5. Jiang, H. & Chan, Y. W. Chromatin bridges: stochastic breakage or regulated resolution? *Trends Genet.* **40**, 69–82 (2024).
6. Steigemann, P. et al. Aurora B-mediated abscission checkpoint protects against tetraploidization. *Cell* **136**, 473–484 (2009).
7. Carlton, J. G., Caballe, A., Agromayor, M., Kloc, M. & Martin-Serrano, J. ESCRT-III governs the Aurora B-mediated abscission checkpoint through CHMP4C. *Science* **336**, 220–225 (2012).
8. Bhowmick, R. et al. The RIF1-PP1 axis controls abscission timing in human cells. *Curr. Biol.* **29**, 1232–1242 e1235 (2019).
9. Petsalaki, E. & Zachos, G. An ATM-CHK2-INCENP pathway prevents chromatin breakage by regulating the abscission checkpoint. *Mol. Cell Oncol.* **8**, 1877999 (2021).
10. Petsalaki, E. & Zachos, G. An ATM-Chk2-INCENP pathway activates the abscission checkpoint. *J. Cell Biol.* **220**, e202008029 (2021).
11. Maciejowski, J., Li, Y., Bosco, N., Campbell, P. J. & de Lange, T. Chromothripsis and kataegis induced by telomere crisis. *Cell* **163**, 1641–1654 (2015).
12. Bennink, M. L. et al. Unfolding individual nucleosomes by stretching single chromatin fibers with optical tweezers. *Nat. Struct. Biol.* **8**, 606–610 (2001).
13. Mihardja, S., Spakowitz, A. J., Zhang, Y. & Bustamante, C. Effect of force on mononucleosomal dynamics. *Proc. Natl. Acad. Sci. USA* **103**, 15871–15876 (2006).
14. Yan, J. et al. Micromanipulation studies of chromatin fibers in *Xenopus* egg extracts reveal ATP-dependent chromatin assembly dynamics. *Mol. Biol. Cell* **18**, 464–474 (2007).
15. Jiang, H., Kong, N., Liu, Z., West, S. C. & Chan, Y. W. Human endonuclease ANKLE1 localizes at the midbody and processes chromatin bridges to prevent DNA damage and cGAS-STING activation. *Adv. Sci. (Weinh.)* **10**, e2204388 (2023).
16. Umbreit, N. T. et al. Mechanisms generating cancer genome complexity from a single cell division error. *Science* **368**, eaba0712 (2020).
17. Janssen, A., van der Burg, M., Szuhai, K., Kops, G. J. & Medema, R. H. Chromosome segregation errors as a cause of DNA damage and structural chromosome aberrations. *Science* **333**, 1895–1898 (2011).
18. Shoshani, O. et al. Chromothripsis drives the evolution of gene amplification in cancer. *Nature* **591**, 137–141 (2021).
19. Hoffelder, D. R. et al. Resolution of anaphase bridges in cancer cells. *Chromosoma* **112**, 389–397 (2004).
20. Tucker, J. B. et al. Misaligned chromosomes are a major source of chromosomal instability in breast cancer. *Cancer Res. Commun.* **3**, 54–65 (2023).
21. Zhang, C. Z. et al. Chromothripsis from DNA damage in micronuclei. *Nature* **522**, 179–184 (2015).
22. Kneissig, M. et al. Micronuclei-based model system reveals functional consequences of chromothripsis in human cells. *Elife* **8**, e50292 (2019).
23. Lee, J. J. et al. ERalpha-associated translocations underlie oncogene amplifications in breast cancer. *Nature* **618**, 1024–1032 (2023).
24. Geng, X. et al. PICH supports embryonic hematopoiesis by suppressing a cGAS-STING-mediated interferon response. *Adv. Sci. (Weinh.)* **9**, e2103837 (2022).
25. Mackenzie, K. J. et al. cGAS surveillance of micronuclei links genome instability to innate immunity. *Nature* **548**, 461–465 (2017).
26. Harding, S. M. et al. Mitotic progression following DNA damage enables pattern recognition within micronuclei. *Nature* **548**, 466–470 (2017).
27. Dou, Z. et al. Cytoplasmic chromatin triggers inflammation in senescence and cancer. *Nature* **550**, 402–406 (2017).
28. Hong, Y. et al. LEM-3 is a midbody-tethered DNA nuclease that resolves chromatin bridges during late mitosis. *Nat. Commun.* **9**, 728 (2018).
29. Hong, Y. et al. The conserved LEM-3/Ankle1 nuclease is involved in the combinatorial regulation of meiotic recombination repair and chromosome segregation in *Caenorhabditis elegans*. *PLoS Genet.* **14**, e1007453 (2018).
30. Song, J. et al. Functional dissection of the conserved *C. elegans* LEM-3/ANKLE1 nuclease reveals a crucial requirement for the LEM-like and GIY-YIG domains for DNA bridge processing. *Nucleic Acids Res.* **53**, gkaf265 (2025).
31. Dittrich, C. M. et al. LEM-3 - A LEM domain containing nuclease involved in the DNA damage response in *C. elegans*. *PLoS ONE* **7**, e24555 (2012).
32. Brachner, A. et al. The endonuclease Ankle1 requires its LEM and GIY-YIG motifs for DNA cleavage in vivo. *J. Cell Sci.* **125**, 1048–1057 (2012).
33. Song, J., Freeman, A. D. J., Knebel, A., Gartner, A. & Lilley, D. M. J. Human ANKLE1 is a nuclease specific for branched DNA. *J. Mol. Biol.* **432**, 5825–5834 (2020).
34. Freeman, A. D. J., Declais, A. C., Wilson, T. J. & Lilley, D. M. J. Biochemical and mechanistic analysis of the cleavage of branched DNA by human ANKLE1. *Nucleic Acids Res.* **51**, 5743–5754 (2023).
35. Braun, J., Meixner, A., Brachner, A. & Foisner, R. The GIY-YIG type endonuclease ankyrin repeat and LEM domain-containing protein 1 (ANKLE1) is dispensable for mouse hematopoiesis. *PLoS ONE* **11**, e0152278 (2016).
36. Wyatt, H. D., Sarbajna, S., Matos, J. & West, S. C. Coordinated actions of SLX1-SLX4 and MUS81-EME1 for Holliday junction resolution in human cells. *Mol. Cell* **52**, 234–247 (2013).
37. Wyatt, H. D., Laister, R. C., Martin, S. R., Arrowsmith, C. H. & West, S. C. The SMX DNA repair tri-nuclease. *Mol. Cell* **65**, 848–860.e811 (2017).
38. Garner, E., Kim, Y., Lach, F. P., Kottemann, M. C. & Smogorzewska, A. Human GEN1 and the SLX4-associated nucleases MUS81 and SLX1 are essential for the resolution of replication-induced Holliday junctions. *Cell Rep.* **5**, 207–215 (2013).
39. Wechsler, T., Newman, S. & West, S. C. Aberrant chromosome morphology in human cells defective for Holliday junction resolution. *Nature* **471**, 642–646 (2011).
40. Sarbajna, S., Davies, D. & West, S. C. Roles of SLX1-SLX4, MUS81-EME1, and GEN1 in avoiding genome instability and mitotic catastrophe. *Genes Dev.* **28**, 1124–1136 (2014).
41. Chan, Y. W., Fugger, K. & West, S. C. Unresolved recombination intermediates lead to ultra-fine anaphase bridges, chromosome breaks and aberrations. *Nat. Cell Biol.* **20**, 92–103 (2018).
42. Tiwari, A., Addis Jones, O. & Chan, K. L. 53BP1 can limit sister-chromatid rupture and rearrangements driven by a distinct ultrafine DNA bridging-breakage process. *Nat. Commun.* **9**, 677 (2018).

43. West, S. C. et al. Resolution of recombination intermediates: mechanisms and regulation. *Cold Spring Harb. Symp. Quant. Biol.* **80**, 103–109 (2015).

44. Ho, H. N. & West, S. C. Generation of double Holliday junction DNAs and their dissolution/resolution within a chromatin context. *Proc. Natl. Acad. Sci. USA* **119**, e2123420119 (2022).

45. Chan, Y. W. & West, S. GEN1 promotes Holliday junction resolution by a coordinated nick and counter-nick mechanism. *Nucleic Acids Res.* **43**, 10882–10892 (2015).

46. Rass, U. et al. Mechanism of Holliday junction resolution by the human GEN1 protein. *Genes Dev.* **24**, 1559–1569 (2010).

47. Lilley, D. M. & Kemper, B. Cruciform-resolvase interactions in supercoiled DNA. *Cell* **36**, 413–422 (1984).

48. Barraud, P. & Allain, F. H. ADAR proteins: double-stranded RNA and Z-DNA binding domains. *Curr. Top. Microbiol. Immunol.* **353**, 35–60 (2012).

49. Strick, T. R., Croquette, V. & Bensimon, D. Single-molecule analysis of DNA uncoiling by a type II topoisomerase. *Nature* **404**, 901–904 (2000).

50. Biebricher, A. et al. PICH: a DNA translocase specially adapted for processing anaphase bridge DNA. *Mol. Cell* **51**, 691–701 (2013).

51. Spakman, D. et al. PICH acts as a force-dependent nucleosome remodeler. *Nat. Commun.* **13**, 7277 (2022).

52. Stasiak, A., Di Capua, E. & Koller, T. Elongation of duplex DNA by recA protein. *J. Mol. Biol.* **151**, 557–564 (1981).

53. Gemmen, G. J., Millin, R. & Smith, D. E. Tension-dependent DNA cleavage by restriction endonucleases: two-site enzymes are “switched off” at low force. *Proc. Natl. Acad. Sci. USA* **103**, 11555–11560 (2006).

54. Vlijm, R. et al. Nucleosome assembly dynamics involve spontaneous fluctuations in the handedness of tetrasomes. *Cell Rep.* **10**, 216–225 (2015).

55. Prunell, A. A topological approach to nucleosome structure and dynamics: the linking number paradox and other issues. *Biophys. J.* **74**, 2531–2544 (1998).

56. Przadowski, P., Przadowska, R. K. & Guertin, M. J. ANKLE1 cleaves mitochondrial DNA and contributes to cancer risk by promoting apoptosis resistance and metabolic dysregulation. *Commun. Biol.* **6**, 231 (2023).

57. Ran, F. A. et al. Genome engineering using the CRISPR-Cas9 system. *Nat. Protoc.* **8**, 2281–2308 (2013).

58. Kong, N. & Chan, Y. W. Protocol for biallelic tagging of an endogenous gene using CRISPR-Cas9 in human cells. *STAR Protoc.* **4**, 102286 (2023).

59. Chan, Y. W. & West, S. C. Spatial control of the GEN1 Holliday junction resolvase ensures genome stability. *Nat. Commun.* **5**, 4844 (2014).

60. Kong, N., Liu, Z. & Chan, Y. W. RIF1 suppresses the formation of single-stranded ultrafine anaphase bridges via protein phosphatase 1. *Cell Rep.* **42**, 112032 (2023).

61. Zhang, X., Chen, H., Fu, H., Doyle, P. S. & Yan, J. Two distinct overstretched DNA structures revealed by single-molecule thermodynamics measurements. *Proc. Natl. Acad. Sci. USA* **109**, 8103–8108 (2012).

62. Efremov, A. K. et al. Transcriptional repressor TrmBL2 from Thermococcus kodakarensis forms filamentous nucleoprotein structures and competes with histones for DNA binding in a salt- and DNA supercoiling-dependent manner. *J. Biol. Chem.* **290**, 15770–15784 (2015).

Acknowledgements

We thank Prof Yan Jie (National University of Singapore) for the valuable discussions of the manuscript. We also thank Wai Hung Sit, Mar-

garet Chui Ling Tse (University of Hong Kong), and Cheng Zhou (Shenzhen Bay Laboratory) for the general technical assistance. Work in Y.W.C.’s laboratory and Y.Z.’s laboratory was supported by the University of Hong Kong, the Hung Hing Ying Physical Sciences Research Fund, and the Research Grant Council of Hong Kong (GRF17119421, C7009-20GF, and C7035-23GF). Work in S.C.W.’s laboratory was supported by the Francis Crick Institute, which receives core funding from Cancer Research UK (CC2098), the UK Medical Research Council (CC2098), and the Wellcome Trust (CC2098), by the European Research Council (ERC-ADG-666400) and the Louis-Jeantet Foundation. Work in A.K.E.’s laboratory was supported by the start-up funds from Shenzhen Bay Laboratory. F.H. is the recipient of the SZBL-HKU Joint PhD scholarship.

Author contributions

H.J., A.K.E., and Y.W.C. designed the study. H.J. carried out cell biology and biochemical experiments. F.H. carried out biochemical and magnetic tweezer experiments. N.K., Y.C.P., and J.L. helped in biochemical and magnetic tweezer experiments. Z.X. and Y.Z. helped in protein purification. R.S. and S.C.W. prepared the DNA substrates. A.K.E. and Y.W.C. supervised the experiments and data analyses. S.C.W., A.K.E., and Y.W.C. prepared the manuscript with contribution from all the authors.

Competing interests

The authors declare no competing interests.

Additional information

Supplementary information The online version contains supplementary material available at <https://doi.org/10.1038/s41467-025-65905-7>.

Correspondence and requests for materials should be addressed to Artem K. Efremov or Ying Wai Chan.

Peer review information *Nature Communications* thanks the anonymous reviewer(s) for their contribution to the peer review of this work. A peer review file is available.

Reprints and permissions information is available at <http://www.nature.com/reprints>

Publisher’s note Springer Nature remains neutral with regard to jurisdictional claims in published maps and institutional affiliations.

Open Access This article is licensed under a Creative Commons Attribution-NonCommercial-NoDerivatives 4.0 International License, which permits any non-commercial use, sharing, distribution and reproduction in any medium or format, as long as you give appropriate credit to the original author(s) and the source, provide a link to the Creative Commons licence, and indicate if you modified the licensed material. You do not have permission under this licence to share adapted material derived from this article or parts of it. The images or other third party material in this article are included in the article’s Creative Commons licence, unless indicated otherwise in a credit line to the material. If material is not included in the article’s Creative Commons licence and your intended use is not permitted by statutory regulation or exceeds the permitted use, you will need to obtain permission directly from the copyright holder. To view a copy of this licence, visit <http://creativecommons.org/licenses/by-nc-nd/4.0/>.

© The Author(s) 2025